UNIVERSITÀ DI PARMA
ARCHIVIO DELLA RICERCA

University of Parma Research Repository

Analysis of Heavy Ion Irradiation Induced Thermal Damage in SiC Schottky Diodes

This is the peer reviewd version of the followng article:

Original
Analysis of Heavy Ion Irradiation Induced Thermal Damage in SiC Schottky Diodes / Abbate, C.; Busatto, G.; Cova, Paolo; Delmonte, Nicola; Giuliani, Francesco; Iannuzzo, F.; Sanseverino, A.; Velardi, F.. - In: IEEE TRANSACTIONS ON NUCLEAR SCIENCE. - ISSN 0018-9499. - 62:1(2015), pp. 202-209. [10.1109/TNS.2014.2387014]

Availability:
This version is available at: 11381/2787271 since: 2021-10-15T18:10:39Z

Publisher:
Institute of Electrical and Electronics Engineers Inc.

Published
DOI:10.1109/TNS.2014.2387014

Terms of use:

Anyone can freely access the full text of works made available as "Open Access". Works made available

Publisher copyright

note finali coverpage

(Article begins on next page)

26 December 2024

Thermal damage in SiC Schottky diodes induced by heavy ion irradiations

C. Abbate[a,b], G. Busatto[a,b,*], P. Cova[c,d], N. Delmonte[c,d], F. Giuliani[c,d], F. Iannuzzo[a,b], A. Sanseverino[a,b], F. Velardi[a,b]

[a]*DIEI - Università degli Studi di Cassino e del Lazio Meridionale, via G. di Biasio, 43 - 03043 Cassino, Italy*

[b]*INFN - Sez. Roma, p.le Aldo Moro, 2 - 00185 Roma, Italy*

[c]*Dipartimento Ingegneria dell'Informazione, University of Parma, viale G.P. Usberti 181/a - 43124 Parma, Italy*

[d]*INFN - Sez. Pavia, via Agostino Bassi, 6 - 27100 Pavia, Italy*

Abstract

A study is presented aimed at describing phenomena involved in Single Event Burnout induced by heavy ion irradiation in SiC Schottky diodes. On the basis of experimental data obtained for ^{79}Br irradiation at different energies, electro-thermal FEM is used to demonstrate that the failure is caused by a strong local increase of the semiconductor temperature. With respect to previous studies the temperature dependent thermal material properties were added. The critical ion energy calculated by this model is in agreement with literature experimental results. The substrate doping dependence of the SEE robustness was analysed, proving the effectiveness of the developed model for device technological improvements.

1. Work motivation and purpose

Silicon Carbide is a promising substitute for Silicon in high-voltage, high-efficiency and high-power density applications, thanks to its superior electrical and thermal properties [1]. The higher melting point and conductivity allow reduced energy losses, higher operating temperatures and the design of a simpler heat sink. Thanks to its higher critical electric field, a SiC device is much thinner with a higher level of doping [2], leading to a lower on-resistance. The higher saturation carrier velocity allows higher speed and higher operating frequencies.

The SiC Schottky diode is the first SiC power device and, actually, the SiC technology permits to commercialize Schottky diodes rated up to 1200 V, a value not reachable with the silicon technology. Some works have been addressed to study the sensitivity of these device, to Single Event Effects, SEE. Unfortunately, SiC Schottky diodes exhibit failure under proton [3] and heavy ion irradiations [4, 5]. Their breakdown was first attributed to the displacement damage-induced current [4] and then to a strong increase of the temperature, which causes a permanent damages to the structure [5].

In this work we present an electro-thermal analysis able to investigate the SEE sensitivity of SiC Schottky diodes. When an ion with sufficient energy penetrates through the whole epitaxial layer, a high electric field is developed in proximity of the Schottky barrier. The intense electric field combined with a high conduction current density causes a power dissipation able to increase the lattice temperature above the SiC melting point leading to the device failure.

The analysis has been conducted by varying the penetration depth of the ion, the volume of the simulated cell, thermal and electrical parameters of the simulated device.

2. Experimental results

The experimental data referred to in this paper are essentially the same as presented in our previous work [6]. Therefore, the data will be summarized here only briefly. 1200 V commercially available Schottky diodes were irradiated with ^{79}Br at 20, 60 and 240 MeV having LET= 43.5, 27.9 and 9.3 MeVcm^2/mg, respectively. The ionization energy loss computed by SRIM [7], for the three cases, is reported in Fig. 1. The schematic of circuit used for biasing and monitoring the Device Under Test, DUT, is reported in Fig. 2.

The DUT, is reverse biased during each irradiation at a fixed voltage by the high voltage

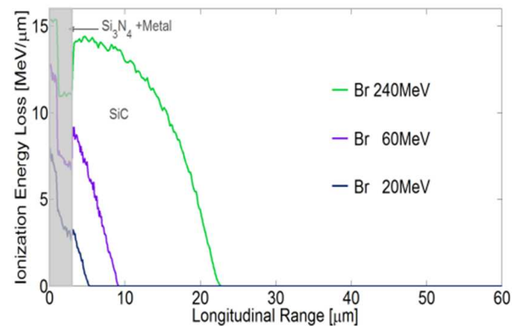

Fig. 1. Ionization energy loss vs longitudinal range of the irradiated ion species.

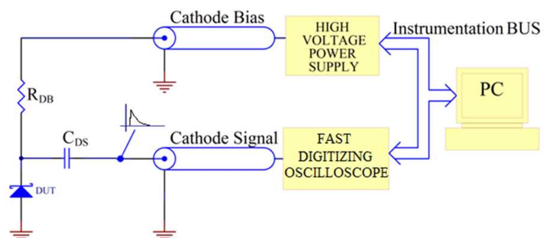

Fig. 2. Schematic of the circuit used during irradiation.

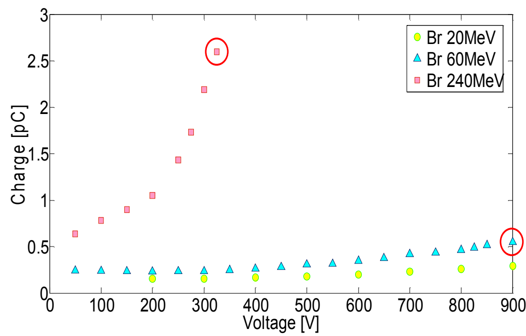

Fig. 3: The collected mean charge vs anode voltage for irradiations

power supply. Each sample is subjected to several irradiations at increasing biasing voltage.

A fixed number of 1500 impacting ions is used for each irradiation. A fast digitizing oscilloscope is used to acquire the current pulses associated with the charge generated during each impact and collected at the cathode terminal. The leakage current is measured before and after each irradiation for verifying if the DUT has been damaged by the irradiation.

Fig. 3 reports the mean value of the charge collected during the impact of ^{79}Br ions at 240 MeV, 60 MeV and 20 MeV, as a function of the anode voltage applied during the irradiation. The ordinates represent the mean value of the charge computed, as the integral of the current pulse collected at the anode terminal, on a population of 1500 events (ions impacting on the device active area). In Fig. 3, the biasing voltage at which permanent damages are observed in the DUT after the irradiation are marked with a red circle. The damages are identified thanks to the increase of at least 30 nA of the leakage current measured after the irradiation. The voltages at which damages are registered are 300 V and 900 V for irradiations with ^{79}Br at 240 MeV, 60 MeV, respectively. No damage was observed after irradiations with ^{79}Br at 20 MeV.

3. Electrical simulations

We performed 3D finite elements ATLAS simulations [8]. The circuit used for the simulations is reported in Fig. 4. We simulate only a portion of the active region of the device in order to reduce the number of mesh points in the 3D structure. We take into account the overall capacitance of the device by means of C_{EQ} in parallel to the structures. L_D accounts for the stray inductance and R_D for the input resistance of the oscilloscope. The power supply V_D describes the coupling capacitors C_{DS} of Fig. 2. The actual parameters of the DUT are not supplied by the manufacturer so we have set the values that are usually used in SiC Schottky diodes with comparable voltage ratings, that is: Metal thickness, $W_{METAL} = 1$ µm, Epitaxial layer thickness, $W_{EPI} = 8$ µm, Epitaxial layer doping, $N_{EPI} = 5\cdot10^{17}$ cm^{-3}, and Substrate doping, $N_{SUB} = 5\cdot10^{18}$ cm^{-3}.

The procedure used for the simulations, described in [9], was adapted for the SiC material. To separate

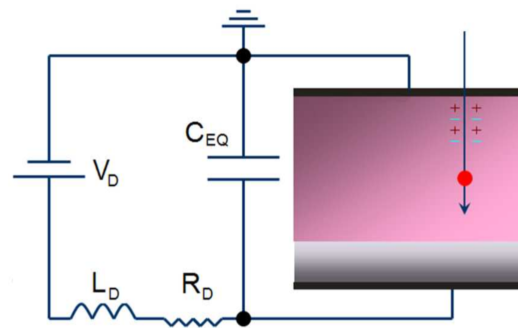

Fig. 4: Schematic of the circuit used for ATLAS simulations.

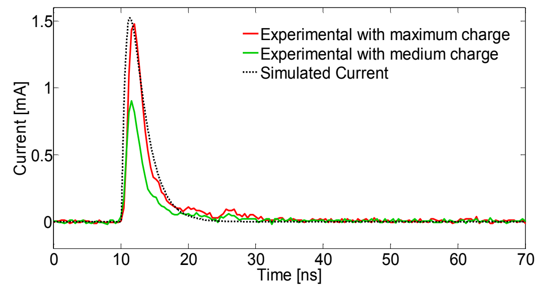

Fig. 5: Experimental and simulated current waveforms for irradiation with ^{79}Br at $V_D = 300$ V. Experimental curves refer to the event with maximum and medium collected charge. Simulation refers to 23 µm penetration depth.

the effects of the range and LET of the impacting particle, we used the same ionization energy at the surface and changed the penetration depth. In particular, for the ^{79}Br at 240 MeV, we used the charge deposited in SiC according to the ionization energy losses computed by SRIM, Fig. 1. For ^{79}Br at 20 and 60 MeV we used the same surface charge deposition and ranges reduced to 4 and 6 µm, respectively.

The simulated waveforms of the current in R_D, corresponding to the input resistance of the oscilloscope, is reported as a dashed line in Fig. 5 for $V_D = 300$ V and 23 µm penetration depth. It is compared with the experimental waveforms related to the events for which we got the maximum and medium values of the collected charge (red and green curves, respectively). The figure reveals a good agreement between simulation and experiment.

The waveforms of the current in the simulated portion of the Schottky diode are reported in Fig. 6, for the three values of the penetration depth and for $V_D = 300$ V. The current peaks become very high and increase with the range of the impacting ion.

The electric field and the current density along the ion track at the instant of the current peak are reported in Figs. 7 a) and b), respectively. Green, blue, and red curves refer to the penetration depths 4, 6, and 23 µm, respectively. For comparison the electric field before the ion strike is reported in black, too. Because of the very large current density, large space charge regions are originated by the carriers moving through current path. These space charge sustain large electric field along the ion track.

Let us consider the case of 23 µm penetration depth for which a current peak of about 1 A is

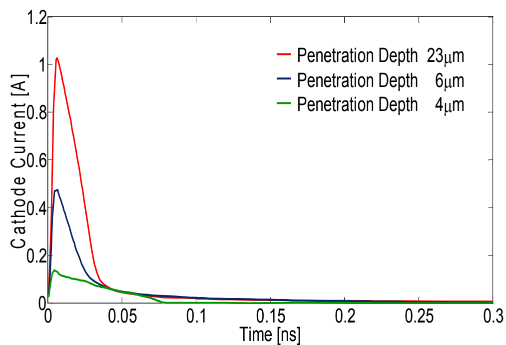

Fig. 6: Current waveforms in the simulated portion of the Schottky diode at V_D = 300 V, for three penetration depths of impacting ions.

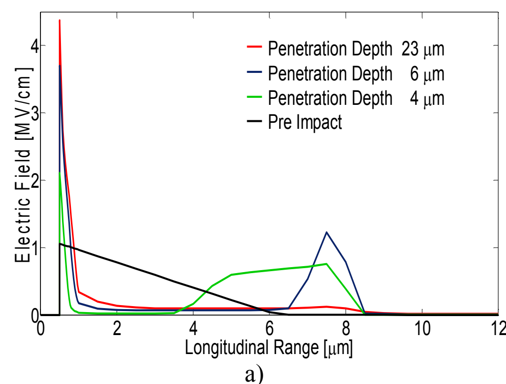

a)

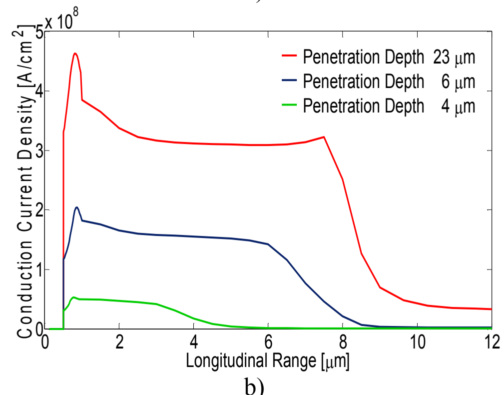

b)

Fig. 7: The electric field a) and the conduction current density b) along the ion track in the Schottky diode, at the instant of the current peak, for V_D = 300 V and for three penetration depths of impacting ions.

observed. Because of the very high conduction current density and electric field, a very large power density is dissipated in the structure, particularly at the Schottky junctions where causes a strong local increase of the temperature, leading to the device failure. The proposed mechanism is very different from the one used to describe the SEB in high voltage Si power PiN diodes [10, 11].

This model applies when the range of the impacting particle is smaller than the thickness of the low-doped region of the device. In this case, the charge deposited by the ion is enough to trigger a time evolution during which a large electric field develops at the N^--N^+ interface. When the biasing voltage is large enough, the peak of the electric field becomes larger than the avalanche field and the

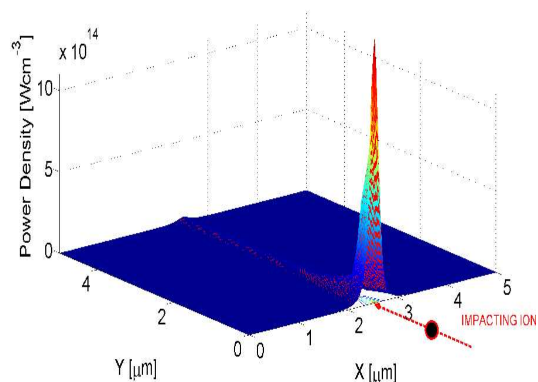

Fig. 8: Power density obtained by ATLAS simulation for V_D = 300 V and 23 μm penetration depth.

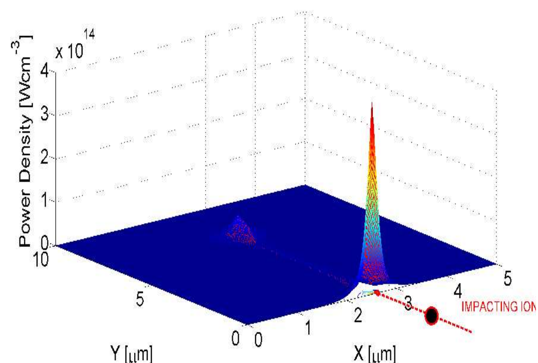

Fig. 9: Power density obtained by ATLAS simulation for V_D = 300 V and 6 μm penetration depth.

conditions for an electric instability are formed causing the device failure.

For obvious reasons, the failure mechanism described in [11] does not apply when the range is larger than the base thickness. But this model does not apply also to the cases when the penetration depths is 4 and 6 μm. In fact, due to the small charge deposited by the particle, the local current density is not enough to cause the electric field at the N^--N^+ interface to become larger than the avalanche field in SiC, which is much larger than in Si. Because of that, we attribute all the failures of Schottky diodes to damages induced to the junction due to its over-heating caused by the local large power dissipation.

The power density along the ion track, at V_D = 300 V, is reported in Figs. 8 and 9 for 23 μm and 6 μm penetration depths, respectively. These data are used as the input of the thermal simulations described in the next section.

4. Thermal simulations

In principle, the ATLAS simulator could be used also for performing electro-thermal simulations. But such a simulation would require very high computational capability and very long execution time. In fact, we have to simulate volumes larger than that used for the electrical simulation, including the temperature dependence of the thermal materials properties, to get the proper accuracy. Consequently, to study the thermal behavior for longer time, taking

1
2
3
4
5
6
7
8
9
10
11
12
13
14
15
16
17
18
19
20
21
22
23
24
25
26
27
28
29
30
31
32
33
34
35
36
37
38
39
40
41
42
43
44
45
46
47
48
49
50
51
52
53
54
55
56
57
58
59
60

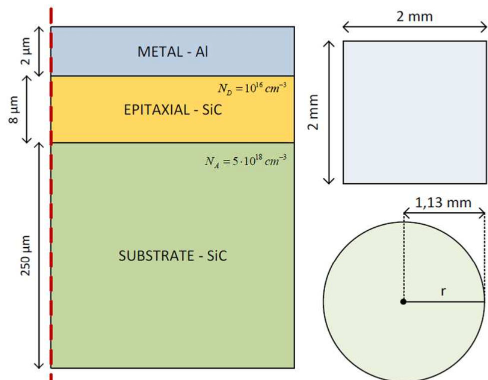

Fig. 10: Rectangle used for generating the cylindrical structure used in the thermal simulations. The base of the cylinder is equivalent to the area of the chip.

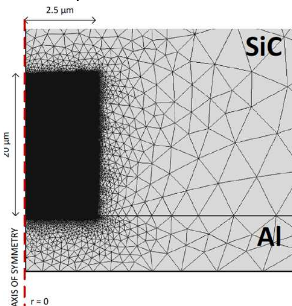

Fig. 11: A detail of the mesh used in thermal simulations.

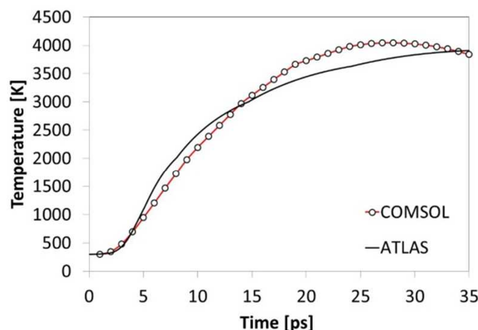

Fig. 12: Comparison between results obtained by ATLAS electro-thermal simulation and COSOL thermal simulation. Simulations refer to 23 μm penetration depth and $V_D = 300$ V [15].

into account the whole 3D chip structure, the thermal connection with the package, and temperature dependent material properties, we built a numerical thermal model using COMSOL Multiphysics [12], exploiting the cylindrical symmetry condition. The rectangle used for generating the cylindrical structure and a detail of the mesh employed in the thermal simulations are reported in Figs. 10 and 11, respectively.

In this model, following a procedure similar to that used in [13, 14], the volumetric heat generation calculated by ATLAS in the first time transient of 35 ps was inserted as a heat flux source, using a two-dimensional time function: Fig. 12 [15] reports the good match obtained with the thermal behavior calculated in the first 35 ps by ATLAS. Fig. 13 shows the 3D thermal map calculated inside the SiC at the time of maximum temperature (26 ps). More

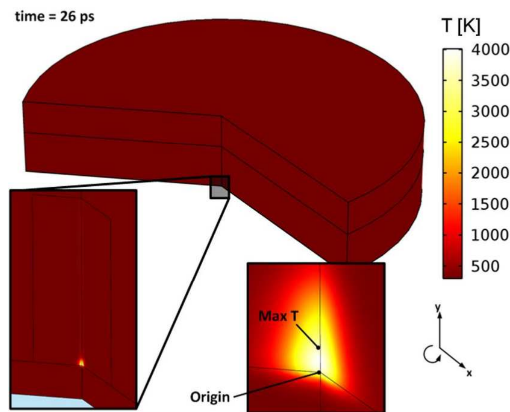

Fig. 13: 3D temperature distribution at the instant when the maximum temperature is reached for 23 μm penetration depth and $V_D = 300$ V.

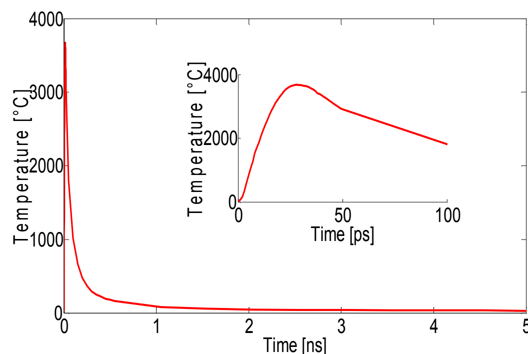

Fig. 14: Evolution of the maximum temperature obtained by COMSOL thermal simulation for 23 μm penetration dept (E = 240 MeV) and $V_D = 300$ V.

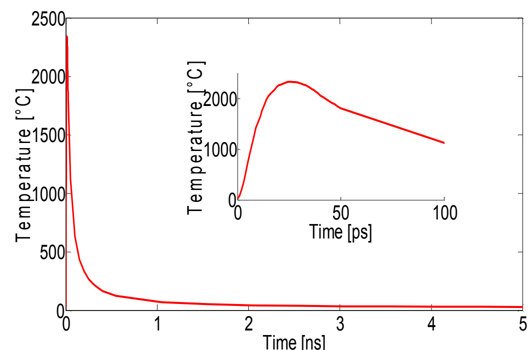

Fig. 15: Evolution of the maximum temperature obtained by COMSOL thermal simulation for 6 μm penetration depth (E = 60 MeV) and $V_D = 300$ V.

details about the model setting procedure can be found in [15].

From Fig. 13 it can be observed that only a very thin portion (about 50 nm) of the 2 mm thick Al layer is interested by heating.

Figs. 14 and 15 show the evolutions of the maximum temperature, for $V_D = 300$ V, in the cases of ion impacts with energy of 240 MeV and 60 MeV, respectively. It is worth to note that, in the first case, where damages were experimentally observed at the DUT (Fig. 3), the temperature becomes larger than the SiC melting point (3100 K) for about 40 ps. In the second case, the temperature is always lower than that limit.

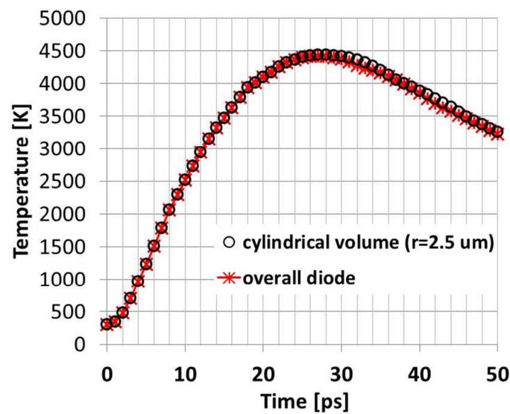

Fig. 16: Comparison between thermal transient in the origin of the cylinder (see Fig. 13, same conditions) obtained by using as simulation domain the whole diode structure and a reduced cylindrical volume with radius r = 2.5 µm.

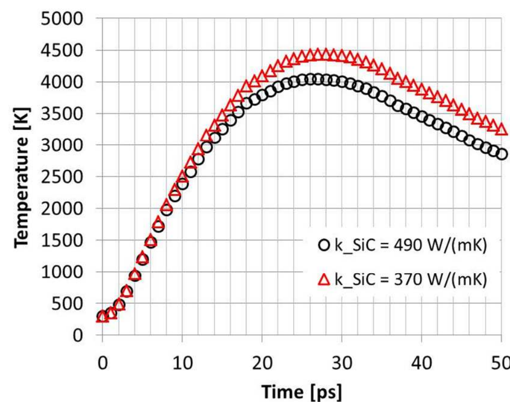

Fig. 17: Comparison between the thermal transient simulated (in the same condition of Fig. 12) for 4H and 6H SiC.

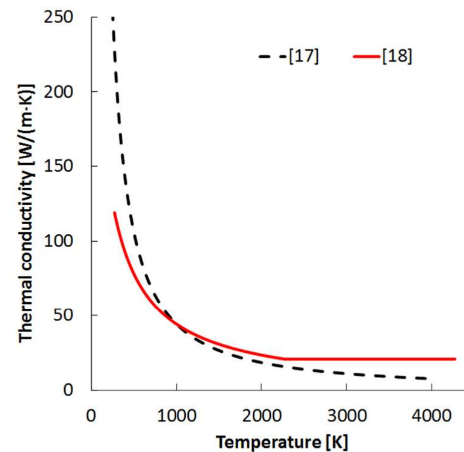

Fig. 18: Thermal behavior of SiC thermal conductivity from [17, 18].

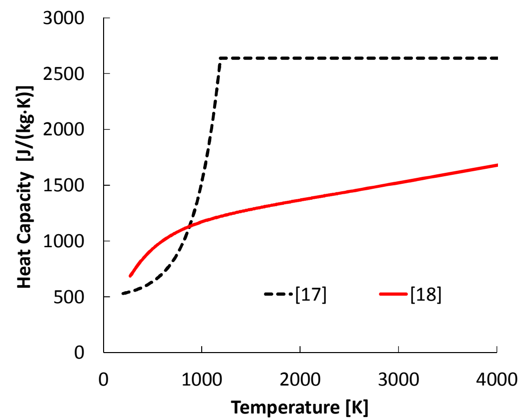

Fig. 19: Thermal behavior of SiC heat capacity from [17, 18] linearly extrapolated above the SiC Debye temperature.

4.1. Analysis on thermally critical volume

Once the ATLAS simulation was reproduced by COMSOL, the analysis of the thermally critical volume to be simulated was conducted, in order to find the minimum portion of the device which has to be simulated to account for the non-adiabatic boundary conditions.

The thermal simulation of the whole SiC Schottky diode structure was preformed, at the same conditions previously described. As can be observed in Fig. 16, a very small difference appears with respect to the cylindrical domain with r = 2.5 µm, only in the cooling phase, after the temperature maximum is reached. This result allows to consider only such a small reduced volume in the following thermal simulation, since the target of the work is to study the time range in which the temperature approaches values close to the semiconductor melting point.

4.2. Comparison between 6H and 4H SiC behavior

The models matching reported in Fig. 12 was related to 6H SiC, which has a thermal conductivity k = 490 W/mK [16]. Since the experimental results reported in Fig. 3 were related to devices made on 4H SiC (k = 370 W/mK [16]), the thermal transient was calculated also with this new value of k. The comparison between the two simulations obtained with COMSOL is reported in Fig. 17, which shows an increase of about 400 K of the maximum temperature in the second case.

4.3. Material parameters thermal dependence

The model considered up to now uses constant thermal conductivity k and heat capacity c_p. The inclusion of the thermal dependence of these two parameters is not an obvious task, since a few data are reported in literature for SiC above 900 K.

Fig. 18 shows the thermal behavior of k for from two research groups (measured for SiC with different crystalline structure and with different techniques) calculated by the formulas reported in [17, 18]. It is important to notice that Wei et al. [17] extracted the formula by interpolating data up to about 900 K on 4H SiC, while Munro et al. [18] performed measurement up to 2200 K, but using semiconductor with different crystal structure.

In both cases k rapidly decreases, reaching values lower than one order of magnitude at the melting point. Similarly, the same authors report formulas for the thermal dependence of the SiC heat capacity, by measurements in the same range as described above.

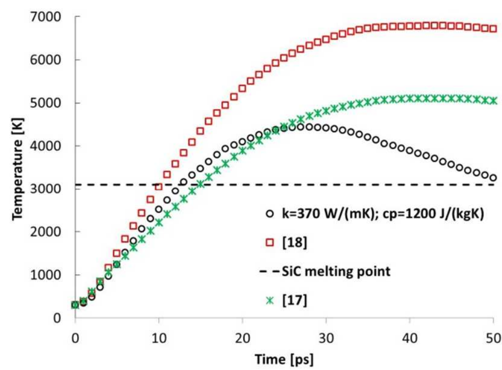

Fig. 20: Comparison between the thermal transient simulated (in the same condition of Fig. 12) with different parameters' models.

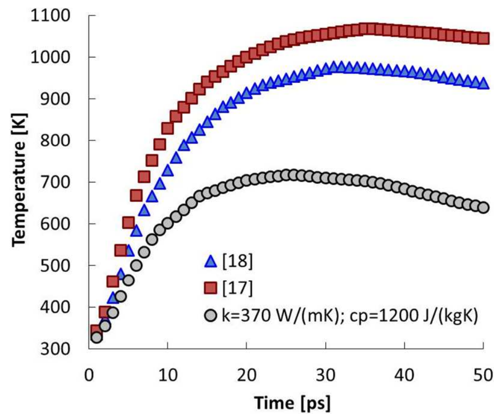

Fig. 21: Comparison between the thermal transient simulated (in the same condition of Fig. 12, but with E = 60 MeV) with different parameters' models.

In this case, as it happens in other semiconductors, we supposed a linear behavior after the Debye temperature [19]. Fig. 19 illustrates these behaviors. In the case of data from [17], due to lack of information, a constant value extrapolation was adopted (worst case for semiconductor heating).

Even though the behavior suggested by [17] is related to 4H SiC, the one from [18] seems to be more effective for our purposes, since it is based on experimental data up to 2200 K. In both cases c_p increases with temperature, then partially compensating the effect of the reduction in k.

By inserting these parameters thermal dependence in the thermal transient simulations, significant variation were observed (Fig. 20), but in all cases the SiC melting point is reached, so confirming the previously obtained results.

Moreover, also the thermal simulation with temperature dependent parameters performed for the case of ion energy of 60 MeV (Fig. 21), confirmed the previous results (maximum temperature much lower than the melting point), in agreement with experimental data.

4.4. Estimation of the melted region dimension

Referring to the device with substrate doping $N_{SUB} = 5{\cdot}10^{18}$ cm^{-3}, E = 240 MeV, V_D = 300 V, the volume where the temperature reaches values larger

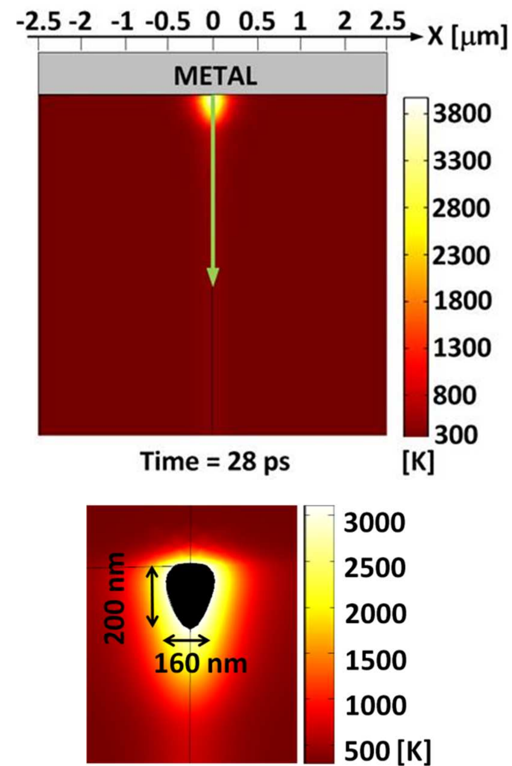

Fig. 22: 2D temperature distribution at the instant of the maximum temperature for 23 µm penetration depth and V_D = 300 V (top); 3D enlargement showing the melted volume (bottom).

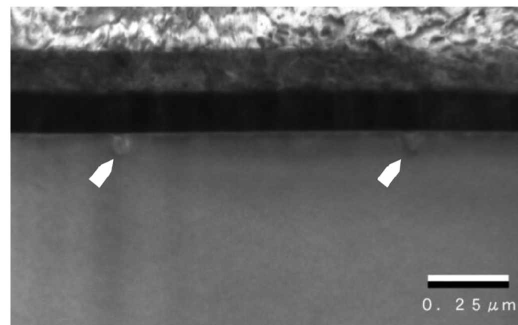

Fig. 23: TEM picture of the damaged areas in a Schottky diode [5].

than SiC melting point in the transient simulations (see Fig. 22) is of the same order of magnitude (100 nm) of the volume where damages were experimentally observed, as shown in Fig. 23, which reports the TEM picture of a SiC Schottky diode after the irradiation, taken from [5]. Such a comparison can be done only qualitatively since, once the melting point is reached, in the fused region the physical properties of the semiconductor are lost and no exact behavior can be evaluated.

4.5. Thermal modeling for diode SEE robustness optimization

The electro-thermal model described above can be exploited to study the dependence of the SiC Schottky diode robustness to SEE by the device structure. Even if the simulated thermal behavior has a large incertitude, it can supply important information by comparing structures with different

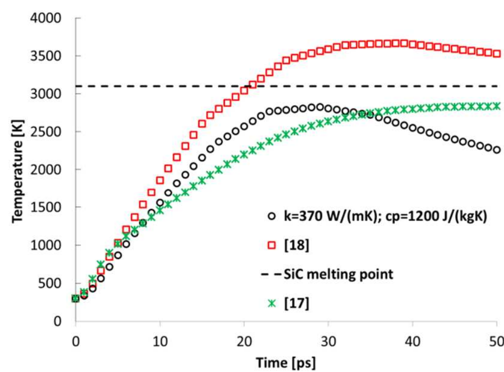

Fig. 24. Comparison between the thermal transient simulated (in the same condition of Fig. 12) with different parameters' models in the case of substrate doping $N_{SUB} = 2.5 \cdot 10^{18}$ cm^{-3}.

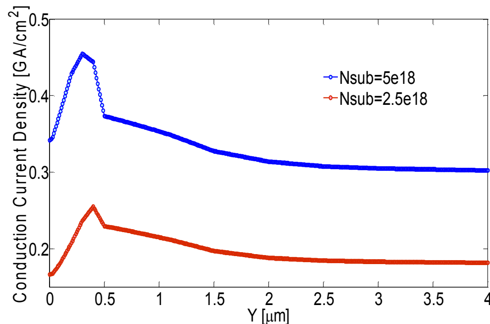

Fig. 25. Conduction current density in the epitaxial layer along the ion track at t = 6.5 ps for $N_{SUB} = 2.5 \cdot 10^{18}$ cm^{-3} and $N_{SUB} = 5 \cdot 10^{18}$ cm^{-3} (E = 240 MeV, V_D = 300 V).

technological parameters.

As an example in [15] the influence of the substrate doping was studied, finding a strong reduction of the maximum temperature in the thermal transient following the ion impact, by reducing the substrate doping by a factor two. This analysis was repeated here by the improved model with thermally dependent parameters k and c_p and the result was partially confirmed, as shown in Fig. 24 (which has to be compared with Fig. 20).

One of the models indicates a maximum temperature above the melting point but, anyway it is reduced to almost half with respect to the case $N_{SUB} = 5 \cdot 10^{18}$ cm^{-3}.

The temperature reduction can be explained by looking at the conduction current density (Fig. 25) at the instant of the maximum power dissipation (t = 6.5 ps, E = 240 MeV and V_D = 300 V) for $N_{SUB} = 5 \cdot 10^{18}$ cm^{-3} and $2.5 \cdot 10^{18}$ cm^{-3}. The substrate doping reduction induces a decrease of the conduction current density, since the portion of substrate not covered by the particle range behaves like a resistor in series with the ion track and the reduction of its doping causes a proportional increase of its resistance. Hence, the current flowing through it is strongly reduced being the applied voltage the same for the two cases. The reduction of this current causes a significant reduction of the conduction current in the ion track being the other components, mainly displacement currents, unchanged.

This result is important, because it highlights the possibility, for the manufacturer of SiC components, to improve the SEE robustness by a proper design the doping profile.

Similarly, other analyses are possible by exploiting the electro-thermal model described in this paper, in order to study the SEE robustness dependence by different technological parameters.

5. Conclusions

An experimental and simulation study about the damages induced by heavy ion irradiation in SiC Schottky diodes has been presented. It is based on electro-thermal and thermal finite element simulations.

The study has demonstrated that, as a consequence of the ion penetrating through the device, the temperature at the Schottky barrier can become bigger than the SiC melting point for a time large enough to cause permanent damages to the SiC lattice.

The analysis has been conducted by varying the penetration depth of the ion, the volume of the simulated cell, thermal and electrical parameters of the simulated device.

The proposed simulation methodology can be very useful for the manufacturer of SiC components, since it can supply indications useful to improve the SEE robustness of these devices.

References

[1] M. Östling et al., "SiC power devices – present status, applications and future perspective", Proc. ISPSD 2011, pp. 10-15.

[2] B.J. Baliga, "Fundamentals of power semiconductor devices", Springer, 2008.

[3] S. Kuboyama et al., "Single-event burnout of silicon carbide Schottky barrier diodes caused by high energy protons", IEEE Trans. Nucl. Sci., vol. 54, pp. 2379-2383, 2007.

[4] L. Scheick et al., "Displacement damage-induced catastrophic second breakdown in silicon carbide Schottky power diodes", IEEE Trans. Nucl. Sci., vol. 51, pp. 3193-3198, 2004.

[5] S. Kuboyama et al., "Anomalous charge collection in silicon carbide Schottky barrier diodes and resulting permanent damage and single-event burnout", IEEE Trans. Nucl. Sci., vol. 53, pp. 3343-3348, 2006.

[6] C. Abbate et al., "Single event effects induced by heavy ion irradiation in SiC power devices", Proc. RADECS 2013.

[7] SRIM (Stopping and Range of Ions in Matter) http://www.srim.org/

[8] ATLAS User's manual. SILVACO International, Santa Clara, CA (USA)

[9] G. Busatto et al., "Experimental study and numerical investigation on the formation of single event gate damages induced on medium voltage power MOSFET", Microelectronics Reliability, vol. 50, issues 9-11, pp. 1842-1847, 2010.

[10] G. Soelkner et al. "Charge carrier avalanche multiplication in high-voltage diodes triggered by ionizing radiation," IEEE Trans. Nucl. Sci., Vol.47, no.6, pp.2365 - 2372, Dec 2000.

[11] A. M. Albadri et al., "Coupled Electro-Thermal Simulations of Single Event Burnout in Power Diodes," IEEE Trans. Nucl. Sci., vol. 52, no. 6, 2194-2199, 2005.

[12] COMSOL Multiphysics®, https://www.comsol.com

[13] P. Cova, et al. “Thermal characterization and modeling of power hybrid converters for distributed power systems”, Microelectronics Reliability, vol. 46, pp. 1760-1765, 2006.
[14] P. Cova, et al. “Thermal modeling of high frequency DC–DC switching modules: electromagnetic and thermal simulation of magnetic components”, Microelectronics Reliability, vol. 48, pp. 1468-1472, 2008.
[15] C. Abbate, G. Busatto, P. Cova, N. Delmonte, F. Giuliani, F. Iannuzzo, A. Sanseverino, F. Velardi, “Thermal damage in SiC Schottky diodes induced by SE heavy ions”, Microelectronics Reliability, vol. 54, 2014 (in press).
[16] S.A. Kukushkin, A.V. Osipov, V.N. Bessolov, B.K. Medvedev, V.K. Nevolin, K.A. Tkarik, “Substrates for epitaxy of gallium nitride: new materials and techniques”, Rev. Adv. Mater. Sci. vol. 17, pp. 1-32, 2008.
[17] R. Wei, S. Song, K. Yang, Y. Cui, Y. Peng, X. Chen, X. Hu, X. Xu, “Thermal conductivity of 4H-SiC single crystals”, Journal of Applied Physics, vol. 113, pp. 053503-1-4, 2013.
[18] R.G. Munro, “Material Propreties of Sintered alpha-SiC”, J. Phys. Chem., vol. 26, n. 5, pp. 1196-1203, 1997.
[19] T.H. Peng, Y.F. Lou, S.F. Jin, W.Y. Wang, W.J. Wang, G. Wang, X.L. Chen, “Debye temperature of 4H-SiC determined by X-ray powder diffraction”, Power Diffraction, vol. 24, n. 4, pp. 311-314, 2009.